ELSEVIER

Journal of Alloys and Compounds 265 (1998) 215–233

Journal of ALLOYS AND COMPOUNDS

Review article

Critical review on the elastic properties of transition metal carbides, nitrides and carbonitrides

C. Kral, W. Lengauer*, D. Rafaja[1], P. Ettmayer

Institute for Chemical Technology of Inorganic Materials, Vienna University of Technology, Getreidemarkt 9/161, A-1060 Vienna, Austria

Received 11 June 1997

Abstract

Presently available data on the elastic properties of transition metal carbides, nitrides and carbonitrides are critically reviewed. It is shown that a lot of information is available on binary systems, but the scatter of the data is quite large, due to different sample preparation methods, different measurement and evaluation methods and insufficient chemical and microstructural characterization of the materials studied. Furthermore, experimental data were used to compare the evaluation methods for Young's modulus as a function of the sample porosity. Only few data are available for ternary and quaternary systems. For the nitrides the elastic constants were determined almost entirely at room temperature only, although the compounds are frequently used at much higher temperatures. Information about the temperature dependency of the carbides is scarce. Therefore, it is obvious that for the design and tailoring of composites additional research work is necessary. © 1998 Elsevier Science S.A.

Keywords: Young's modulus; Poisson ratio; Thin films; Bulk samples; Porosity

1. Introduction

Transition metal carbides, nitrides and carbonitrides are a very interesting class of compounds because they have a unique combination of physical properties such as high melting points, high hardness values, high electrical and thermal conductivities and metallic luster [1–4]. These properties have attracted considerable interest for both technical applications and fundamental studies. The carbides, e.g., WC and TiC, the nitrides, e.g., TiN, and the carbonitrides, e.g., Ti(C,N) are extensively used as hard constituents in metal matrix composites (hardmetals) and in the form of layers (coatings) on cutting tools. In addition, they have a high potential for a variety of other applications such as electrically conducting diffusion barriers in electronic devices, in coatings for solar applications [5–7], as well as for corrosion protection [8].

The mechanical characteristics of hard constituents critically influence the performance of composites, because they are subjected to loads not only at ambient temperatures, and their response to load and temperature cycling will be decisive. Therefore, Young's modulus, Poisson ratio, shear and bulk modulus are most important.

An extensive literature review on the present knowledge of the elastic properties of transition metal carbides, nitrides and carbonitrides has been performed, also with emphasis on the high-temperature properties and the evaluation methods, which is reported here. Furthermore, the differences of Young's modulus between film and bulk samples were compared.

2. Form of the samples

2.1. Bulk samples

Bulk samples are either prepared from their powders by hot-pressing, hot-isostatic-pressing (hiping) and self-propagating high-temperature synthesis (SHS) or from compact metals applying diffusion processes. The advantage of the preparation of the samples from their powders is that a lot of samples that are different in composition and porosity can be made in a relatively short time. The disadvantage of hot-pressing and hiping is that an inert atmosphere, or for the preparation of the nitrides a nitrogen atmosphere, has to be applied to avoid oxidation. A relatively high temperature (2200–3000 K) and pressure is needed to prepare

*Corresponding author. e-mail: wl@metec3.tuwien.ac.at

[1]Permanent address: Dept. of Semiconductor Physics, Charles University, Ke Karlovu 5, CZ-121 16 Prague 2, Czech Republic.

PII S0925-8388(97)00297-1

nearly compact materials by hot-pressing. Therefore impurities are often included which change the material properties considerably. Because of the high porosity obtained by using the SHS technique, it should not be applied for the preparation of transition metal carbides, nitrides and carbonitrides.

To obtain non-porous samples diffusion annealing of transition metals in carbon powder or a nitrogen atmosphere can be applied. But the preparation is time consuming and only small specimens can be received. Furthermore, the texture and the porosity in the center of the sample caused by the diffusion process have to be considered.

2.2. Thin films

2.2.1. PVD

The preparation of layers using physical vapor deposition (PVD) is due to a material transport between the target, which provides the material necessary for the layer preparation, and the substrate. The ejection of the source material is due to a bombardment of the surface of the target with highly energetic gas ions, e.g., Ar^+, accelerated by high voltage. Particles of atomic dimensions are expelled as a result of the momentum transfer between incident ions and the target. The ejected particles traverse the vacuum chamber and are subsequently deposited on a substrate as a thin film. During the last few years various techniques of physical vapor deposition methods have been developed like diode, triode, magnetron and reactive sputtering (see also Section 6.2.2), where thin film growth already at low temperatures and pressure occurs (e.g., suitable for coating the steel substrates). Due to the fact that many different PVD techniques can be applied which do generally not result in layers of near-thermodynamic equilibrium a large scatter in the reported microstructures and properties occurs.

2.2.2. CVD

Chemical vapor deposition (CVD) is the reaction to form the desired compound by the nucleation of the compound or compounds from the gaseous phase onto a substrate where reaction occurs to produce a solid deposit. The compound bearing the deposit material is vaporized, if not already a gas, by either a pressure differential or the action of a carrier gas and is transported to the substrate. Generally the deposition process is either a thermal decomposition or a chemical reduction. Both thermal decomposition as well as chemical reduction involve organometallic compounds, halides and other simple inorganic compounds. CVD processes are dependent on the thermodynamics and the kinetics of the reaction. Even though the formation of a material is thermodynamically feasible, its growth rate must not be too low. For the growth of CVD films temperatures in the region of about 1273 to 2573 K are applied. The CVD process finds its greatest application in the preparation of coatings that are not easily applied by PVD techniques. The advantages of CVD are that

1. various kinds of coatings are possible (carbides, nitrides, oxides, . . .),
2. the crystal growth is controlled by the setting of the reactive gas concentrations,
3. high deposition rates are possible,
4. the state of the coating is closer to thermodynamic equilibrium than the state of PVD layers, i.e. the lattice parameters, occupancy of lattice sites, metalloid contents,
5. the density is close to that of bulk and high-temperature annealed sample material.

However, also in CVD layers the layer–substrate interaction occurs superimposing stresses into the hard phases then influencing their apparent properties (Young's modulus, hardness) and the disadvantages include furthermore that:

1. rather high temperatures are necessary to obtain certain compounds,
2. low pressures restrict the types of substrate that can be coated,
3. a uniform heating of the substrate is sometimes difficult,
4. because of the design of the reactor the uniform coating of complex shapes is difficult.

In Fig. 1, which shows Young's modulus of TiN_{1-x} as a function of the [N]/[Ti] ratio, it can be easily seen that the preparation method definitely influences the elastic prop-

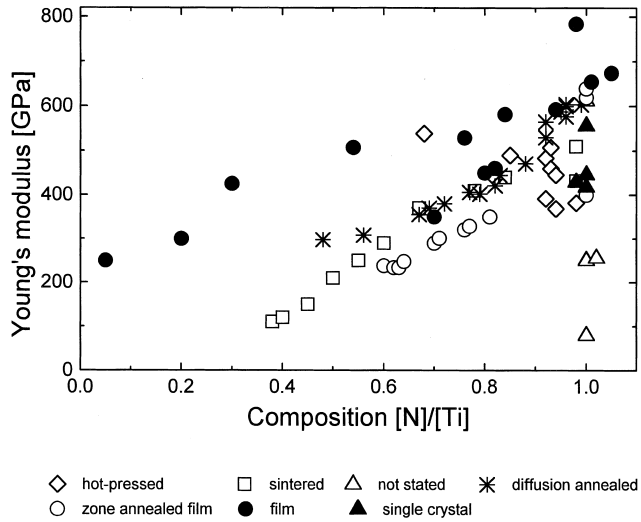

Fig. 1. Young's modulus of titanium nitride as a function of the nitrogen content. Different behavior of the Young's modulus vs. [N]/[Ti] depending on the preparation method can be observed.

erties measured. Young's moduli obtained for bulk samples are generally lower than those for film samples. This might be due to the influence of the substrate, the interaction between substrate and coating, and the stresses occurring in the coating.

3. Characterization of sample material

The information available on the elastic properties are rather inconsistent and contradictory such as for the Ti–N, Zr–N, Ti–C and Nb–C systems. Information on other carbide, nitride and carbonitride systems is rather scarce or altogether lacking. The data differ, in some cases seriously or even contradict each other, due to different and sometimes insufficient chemical and microstructural characterization (chemical analysis of carbon, nitrogen and oxygen, porosity and pore shape, phase analysis, grain size and orientation).

If some materials cannot be prepared in ''zero-porosity'' state, accurate measurement of the porosity is important. Furthermore, as there are different equations for correcting the porosities, a variety of samples with a different amount of porosity would be desirable in order to extrapolate to the zero-porosity state (see Section 5). This has only been performed for a very few compounds, because porosity measurements are time-consuming and difficult.

If the sample is single phase or the amount of phases is well known and the occupancies of the lattice sites or the vacancy concentrations are well defined, a comparison of the measured density by the Archimedes method with X-ray density can be performed.

In case the theoretical density is not known and cannot be calculated, because the occupancy of the lattice sites is not exactly known, metallographic investigations can be done. This is however difficult, because the surface of the samples must be free of artifacts that have been created by the grinding and polishing procedure. This is especially difficult for the class of compounds discussed here, because of their brittle behavior.

A third and quite new method is the investigation of porosity by acoustic microscopy. The advantage of this method is that not the surface, but the interior of the sample is scanned by sound. The depth of the investigation is dependent on the applied frequency. The lower the frequency the higher is the penetration depth and a deeper insight into the material is possible. However, the lower the frequency the lower is the resolution of the technique so that small pores cannot be detected. In practice, it is favorable to polish the surface to obtain a quality which is also suited for any other metallographic investigation (to be able to investigate also the presence of phases, impurity precipitations, grain boundary structure, . . .) and then to apply a higher frequency, e.g., 1 GHz, in acoustic microscopical measurements. This provides a detection of pores down to a few tenths of a μm in a depth of about 10 μm which is appropriate for the investigation of porosity of the present kind of materials.

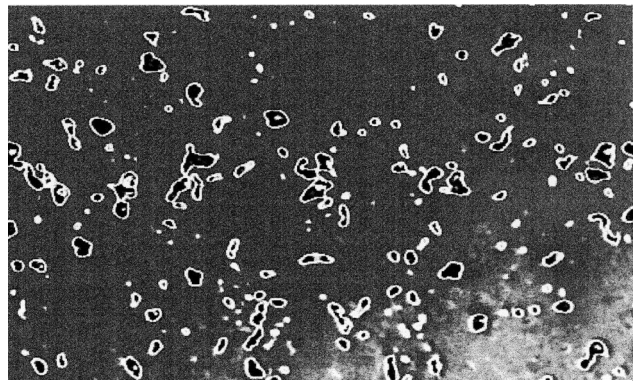

Fig. 2. Acoustic microscope image of an HfCN sample (size: 200 μm×100 μm; 1 GHz; depth: −10 μm; KSI SAM 2000, Krämer Scientific Instruments, Germany).

Fig. 2 shows an acoustic microscope image of a HfCN sample. The pores are dark and the evaluation of porosity with image processing tools (10.4%) gave good agreement with density measurements (9.91%). Surface effects, like grinding and polishing artifacts, do not interfere with this method. The pores can also be detected if different phases are present.

4. Measurement methods of elastic properties

4.1. Evaluation of sound velocity measurements

Because of the extreme brittleness of the samples and the difficult and time-consuming preparation methods mostly sound measurements are employed with the advantage that they are non-destructive. There are three different methods in use. The phase-comparison method [9], the phase-detection method [10] and the pulse-echo overlap (PEO) method [11]. The choice of the method is governed by the thickness of the sample and the desired precision and accuracy of the measurements. However, for any method chosen, the sample porosity always drastically influences the measurements. Wolf [12] showed that porosities of less than 5% have to be achieved to obtain appropriate results as Young's modulus is always calculated for the non-porous state. For the porosity correction of Young's modulus several equations have been proposed [13–18], but they have not been compared yet.

To calculate the elastic properties from the measured sound velocities it is important that the longitudinal as well as the shear velocity is taken into account to get precise and accurate data for Young's modulus and the Poisson ratio. This is due to the fact that without the data of the shear velocity only estimated data can be taken for the Poisson ratio to calculate Young's modulus. In the PEO method the wave velocity (V) is computed from the

''resonance'' relation: a series of wave trains to the transducer (X-cut for longitudinal waves and Y-cut for shear waves) that is acoustically coupled to a buffer rod:

$$V = \frac{2tf_n}{n} \tag{1}$$

where f_n is the ''in phase'' frequency, t is the specimen thickness, n equals the number of wavelengths in $2t$ and $2t/n$ equals λ, the wavelength. For isotropic solids, the elastic moduli are calculated from the measured values of longitudinal (V_p) and shear velocities (V_s) using the following relations:

$$K_s = \rho\left(V_p^2 - \frac{4}{3}V_s^2\right) \tag{2}$$

where K_s is the adiabatic bulk modulus and ρ the density of the sample,

$$G = \rho V_s^2 \tag{3}$$

where G is the shear modulus,

$$E = \frac{9KG}{3K + G)} \tag{4}$$

where E is Young's modulus and

$$v = \left(\frac{E}{2G}\right) - 1 \tag{5}$$

where v is the Poisson ratio. These expressions, Eqs. (1)–(5), hold for isotropic materials.

4.2. Mechanical and XRD investigations

4.2.1. Four-point bending test

A mechanical way to investigate the elastic properties of composites is the four-point bending test. The specimen is mounted in a test device and a bending load, measured, e.g., by a load cell, is applied in certain steps (e.g., 500 N). The deflection of the sample is then measured at the center of the specimen. The strain (ε) at the outer surface of the sample is given, for example, in [19] by

$$\varepsilon(y) = \frac{y}{R} \tag{6}$$

where y is the distance from the neutral axis to the outer surface of the specimen and R is the radius of the circle formed by the bent specimen.

$$\frac{1}{R} = \frac{M}{EI} \tag{7}$$

where M is the moment working on the sample due to the force (F) and the moment arm (r) applied. E represents Young's modulus and I the moment of inertia. For a composite material

$$EI = E_S I_S + E_C I_C \tag{8}$$

where the subscripts S and C stand for the substrate and the coating. Substituting Eq. (7) and Eq. (8) into Eq. (6) results in Eq. (9)

$$\varepsilon(y) = \frac{Fry}{E_S I_S + E_C I_C}. \tag{9}$$

This strain equation is the same for the substrate and the coating. The moment of inertia for the substrate and the coating is given by

$$I_S = \frac{\pi d^4}{64} \tag{10}$$

$$I_C = \frac{\pi}{64}(D^4 - d^4) \tag{11}$$

where D is the diameter of the coated specimen and d is the diameter of the substrate. Because the contribution of I_C due to the term $(D^4 - d^4)$ is negligible for a small coating thickness, the value y at the calculation of $\varepsilon(y)$ can be estimated to be $\frac{1}{2}d$. Therefore the strain becomes

$$\varepsilon = \frac{32Fr}{E_S \pi d^3}. \tag{12}$$

Because of the different elastic properties between the substrate and the coating the stresses are different in contrast to the strains which are the same during loading. For stresses in the coating and the substrate with variable force the following equations can be used.

$$\sigma_S = \frac{32Fr}{\pi d^3} \tag{13}$$

$$\sigma_C = \left(\frac{E_C}{E_S}\right)\frac{32Fr}{\pi d^3}. \tag{14}$$

By the measurement of the deflection (h) at each corresponding load the strain in the coating or the substrate can be estimated.

$$\varepsilon_C = \frac{12hd}{3b^2 - 4a^2} \tag{15}$$

where d is the diameter of the sample and a and b are the inner and outer supporting point distances, respectively.

4.2.2. The $\sin^2\Psi$-method

X-Ray diffraction (XRD) is a non-destructive method suitable for the residual stress investigations. However, only elastic deformations can directly be obtained from the diffraction pattern, not the residual stress. Thus, the relationship between the elastic deformation and the residual stress in the respective material must be known, which is usually expressed in terms of the X-ray elastic constants (XECs). The XECs are related to the material characteristics, namely to the Poisson ratio and to Young's modulus, which can be achieved using another experimental technique. On the other hand, the XECs can be directly obtained from the XRD measurements if a known force is applied on the sample to bend or stretch it. In such a case,

the XRD is a powerful tool to determine the lattice deformation with extremely high precision.

In the residual stress measurement using the XRD two fundamental methods are established. The first one performs the measurement of lattice deformation on a single family of crystallographic planes. In this case, the sample is inclined to reach different angles between the sample surface normal and the diffraction vector. This method is applicable for all materials disregarding their crystal structure, but it is not suitable for the residual stress investigations in the samples, in which a gradient of the mechanical properties is expected. The reason is that the diffraction pattern contains information from different depth below the sample surface, as the penetration depth of the X-ray radiation depends on the inclination of the sample:

$$\tau = \frac{\sin(\Theta - \Psi)\sin(\Theta + \Psi)}{\mu[\sin(\Theta - \Psi) + \sin(\Theta + \Psi)]} \tag{16}$$

where Θ is the diffraction angle, Ψ the angle between the sample surface normal and the diffraction vector, and μ the linear absorption coefficient. This disadvantage can be removed when using an experimental set-up with a small and constant angle of incidence γ, e.g., the Seemann–Bohlin diffractometer or the parallel beam optics. The angle of incidence is typically set between 1 and 10 °. In that case, the penetration depth remains nearly constant for diffraction angles between 30 and 150 ° as it follows from:

$$\tau = \frac{\sin\gamma\sin(2\Theta - \gamma)}{\mu[\sin\gamma + \sin(2\Theta - \gamma)]}. \tag{17}$$

Furthermore, the penetration depth can be adjusted by varying the angle of incidence [20]. The relationship between the lattice deformation ε and the residual stress σ_{ij} is expressed by:

$$\begin{aligned}\varepsilon_{\varphi\psi}(hkl) = {} & 1/2S_2(hkl)(\sigma_{11}\cos^2\varphi + \sigma_{12}\sin 2\varphi \\ & + \sigma_{22}\sin^2\varphi - \sigma_{33})\sin^2\psi + 1/2S_2(hkl)\sigma_{33} \\ & + S_1(hkl)(\sigma_{11} + \sigma_{22} + \sigma_{33}) \\ & + 1/2S_2(hkl)(\sigma_{13}\cos\varphi + \sigma_{23}\sin\varphi)\sin^2\psi.\end{aligned} \tag{18}$$

Models published by Voigt, Reuß and Kröner [21] offer the relationship between the polycrystalline XECs and the XECs obtained from the measurements done with single crystals. The differences in the models are the following: Voigt assumed a constant (averaged) lattice deformation in adjacent grains, which is independent of the crystallographic direction. Consequently, the XEC's calculated from the Voigt model are orientation independent as well. On the contrary, Reuß assumed a homogeneous distribution of the residual stress in the material, which causes unlike lattice deformation in grains, according to their crystallographic orientation. The result of the Kröner's model is, in fact, an average between the two preceding ones.

For practical applications, the relationship between the residual stress and the strain (the lattice deformation) is usually simplified assuming that the residual stress is bi-axial ($\sigma_{13} = \sigma_{23} = \sigma_{33} = 0$) and symmetrical ($\sigma_{11} = \sigma_{22} = \sigma$; $\sigma_{12} = 0$):

$$\varepsilon_{\varphi\psi}(hkl) = [1/2S_2(hkl)\sin^2\psi + S_1(hkl)]\sigma \tag{19}$$

The quality of XRD residual stress measurement is always influenced by the accuracy in determining the positions of the diffraction lines. As it follows from the total differential of the Bragg equation the error in the interplanar spacing is proportional to the cotangent of the diffraction angle and therefore the high-angle diffraction lines are more appropriate for the residual stress measurement than the low-angle diffractions. The problem is that the high-angle diffraction lines are often very weak or even missing.

Two kinds of errors arise determining the line positions. The first one is due to the angular dependent intensity factors (Lorentz, polarisation and absorption), which can shift the respective diffraction line especially in the regions, where the intensity factors change strongly with the diffraction angle. Nevertheless, this shift is mostly negligible. The major contribution to the line shift is caused by the alignment of the diffractometer and its amount depends strongly on the diffraction geometry [22,23]. The most serious sources of instrumental aberrations are the shift of the zero point of the diffractometer, the sample displacement from the focusing circle, sample transparency and sample flatness. If the parallel beam optics were employed only the first instrumental aberration can occur.

4.3. Computational investigations

There is also some computational way to investigate the elastic properties. Miodownik [24] calculated Young's modulus of transition metal carbides from their assessed thermal properties relying on the relationships between elastic and thermal properties [25]. It is important to note that the values can be calculated for any compound irrespective of whether or not it actually occurs in the respective system (see Section 6.1).

Timofeeva et al. [26] calculated Young's modulus applying the equation proposed by Frenkel [27] using the thermal expansion coefficient:

$$E = \left(\frac{k}{R_0^3}\right)\alpha \tag{20}$$

where E is the normal elastic modulus, k the Boltzman constant and R_0 the equilibrium interatomic distance.

5. Porosity corrections

5.1. Equations proposed for porosity correction

Hasselman [13] assumes that the dependency of Young's modulus on the porosity for a continuous phase containing voids as a dispersed phase of spherical shape like polycrystalline refractory materials can be written in the form of the following equation

$$E = E_0\left[1 + \frac{AP}{1-(A+1)P}\right] \tag{21}$$

where E is Young's modulus of the composite, E_0 Young's modulus at zero-porosity, P the volume fraction porosity and A a statistically evaluated constant. The unknown parameters E_0 and A are to be determined from experimental data using, e.g., the non-linear least-square method. According to Hasselman [13] this formula can be applied over the whole porosity range by evaluating the constant A. Many cases might be found where an increase in porosity is accompanied by a change in microstructure (e.g., grain shape and size distribution) or in type of porosity (e.g., change from connected to disconnected pores upon increase of porosity). The porosity dependence of the elastic properties cannot be expressed by a single equation valid over the total range of porosity.

Ondracek [14] developed the following equations

$$E_p^{(1)} = E_{\mathrm{m}}\left[1 - \pi^3\sqrt{\frac{9P^2}{16\pi^2}\frac{z}{x}}\sqrt{1+\left[\left(\frac{x}{z}\right)^2 - 1\right]\cos^2\alpha_{\mathrm{D}}}\right] \tag{22}$$

$$E_{\mathrm{p}}^{(1)} = E_{\mathrm{m}}[1 - 1.21P^{2/3}] \text{ for } P \leq 0.5 \text{ and spherical pores,} \tag{23}$$

where $E_{\mathrm{p}}^{(1)}$ is Young's modulus of the porous material, E_{m} Young's modulus at zero porosity, z and x the rotation and the minor axis of the substituting spheroidal pores, z/x the shape factor, P the porosity (concentration factor) and $\cos^2\alpha_{\mathrm{D}}$ the orientation factor of the spheroidal pores, respectively. Ondracek [14] has chosen a spheroidal model for his assumptions.

By this way the real microstructure of a two-phase material is modeled by a microstructure containing spheroidal pores. This mathematical procedure leads to a preliminary model equation for Young's modulus which, as an engineering approach, is not developed as far as for the conductivity, but reliable up to about 50% by volume of the pores. Its simplified form, valid for big differences between the moduli of the phases is presented in Eqs. (22) and (23).

A different way to calculate the porosity dependence of Young's modulus was chosen by Kupkova [15]. In contrast to the majority of existing more or less theoretical derivations of Young's modulus–porosity relation, which are based on defining an expression for the relation between stress and deformation, the sound velocity as a function of porosity has been calculated and the following relation between Young's modulus and porosity was obtained

$$E = E_0\frac{1 + aP + bP^2}{1 + cP} \tag{24}$$

where E and E_0 represent Young's modulus at porosity P and $P=0$, respectively, and a, b, c are constants independent of porosity, but dependent on the shape and size of the average pore as well as on the properties of the investigated material. It was assumed that the pores are mutually uncorrelated, that they have the same size and form and that they are randomly distributed in a homogeneous matrix. A change of porosity would mean a change of the number of pores, while their form and size remain unchanged.

The equation presented by Wang [16]

$$E = E_0\exp[-(bP + cP^2)] \tag{25}$$

takes into consideration that the dispersed second phase is not of specific shape, orientation and content. Especially for porous materials prepared by hot-pressing, hot-isostatic-pressing and sintering, theories apply much better which take interconnected pores into account, where E is Young's modulus, E_0 is Young's modulus at zero-porosity, b and c are non-negative material constants and P is the porosity. Wang's model is highly idealized with many assumptions (e.g., monosized powder and grain size distribution, simple cubic lattice). However, experimental studies on porous alumina [28], where not only the porosity percentage changed, but also changes from a disconnected to a connected pore structure occurred, were made in order to determine if the equation proposed can satisfactorily describe non-ideal real systems. Wang [16] reports that the extrapolation of Young's modulus for the non-porous state should be made only from a sufficient number of low-porosity specimens, preferably containing less than 5% porosity (see Wolf [12]). The extrapolation of high-porosity data to zero porosity should be avoided. The data obtained by Wang [28] are in good agreement with literature data and his equation is even useable for samples with non-spherical pores, because densification leads to a deviation from the particle's original shape, converting it into a polyhedron. However, the difference between a spherical particle and a non-spherical particle becomes less and less distinguishable when both approach polyhedrons during densification.

Several papers on the porosity dependence of Young's modulus and the ultrasonic velocity have been published by Phani et al. [17,29,30]. He proposed the semi-empirical Eq. (26) of the following form describing the porosity-dependence of Young's modulus of brittle solids

$$E = E_0(1 - aP)^n \quad (26)$$

where E and E_0 are Young's modulus at porosity P and at zero-porosity, where a and n represent material constants. The material constant a may be defined as the ''packing geometry factor'', whose value lies between 1 and 3.85. The second material constant n is dependent on the grain morphology and pore geometry of the material. Eq. (26) presented by Phani et al. [17] is capable of treating the transition of the pore structure from interconnected to isolated, like the equation proposed by Wang [16] (see Eq. (25)). According to Phani et al. [17] it has no limitation with regard to its applicability over any range of porosity. Data obtained by Phani et al. [17] were in good agreement with data presented in literature.

5.2. Comparison of porosity correction methods

Eqs. (21), (23)–(26), (28) (see Section 6.1) have been compared using the data measured by Speck et al. [31] for $NbC_{0.97}$ and the data obtained by Wolf [12] for δ-TiN and δ-ZrN. The free parameters of the respective model were obtained from the non-linear least-square calculation performed with the use of Matlab®. The parameters obtained are presented in Table 1. In Fig. 3 a representative output is given for $NbC_{0.97}$. It can be seen that the experimental data form a Gaussian curve where the equations proposed by Wang [16] (Eq. (25)), Phani [17] (Eq. (26)) and Kupkova [15] (Eq. (24)) fit best in contrast to the evaluation formulas proposed by Hasselman [13] (Eq. (21)) and Ondracek [14] (Eq. (23)) and the one used by Frantsevich [32] (Eq. (28)). However, the parameters a, b, c introduced by Kupkova [15] correlate strongly. That is why the parameter c has not been alternated during the calculation. The output is almost identical to the one obtained by Wang's [16] formula (Eq. (25)). The evaluation formula proposed by Phani [17] (Eq. (26)), e.g., fits best for the Ti–N system, but for the Hf–N system the parameter n has to be odd. In Table 1 it can be seen that the parameters necessary for the calculation of Young's

Table 1
Free parameters obtained from the non-linear least-square fit

	NbC	TiN	HfN
Hasselman [13]			
E_0	549.06±0.6	471.07±0.99	355.1±0.36
A	−4.3220±0.0005	−3.805±0.002	−3.3017±0.002
Ondracek [14]			
E_0	507.98	458.03	375
Kupkova [15]			
E_0	506.5±3.1	448±1.4	343.86±2.2
a	6.29±0.01	−0.2182±0.0078	−22.5±0.8
b	−23.9±0.2	−12.91±0.315	−66.4±1.7
c	8.3±0.5	1	30
Wang [16]			
E_0	505.6±2.0	446.5±1.5	347.0±1
b	1.973±0.005	0.8543±0.0093	1.96±0.02
c	7.8±0.1	17.66±0.38	4.04±0.29
Phani [17]			
$n=0.4$			
E_0	493.07±0.14	451.1±0.5	
a	4.2693±0.00001	4.9372±0.0003	
$n=0.5$			
E_0	499.4±0.16	457.5±0.6	
a	3.8756±0.00001	4.4125±0.0004	
$n=1$			
E_0	515.4±0.2	446.2±0.7	347.7±0.25
a	2.5818±0.00001	2.7777±0.0003	2.1011±0.0002
$n=3$			
E_0			351.3±0.3
a			0.8814±0.00001
$n=5$			
E_0			352.1±0.3
a			0.555±0.0001
Frantsevich [32]			
E_0	527.1±0.2	467.0±0.4	359.1±0.2
a	17.1±0.02	1380±680	8.06±0.05
b	2.35±0.05	4.50	2.35

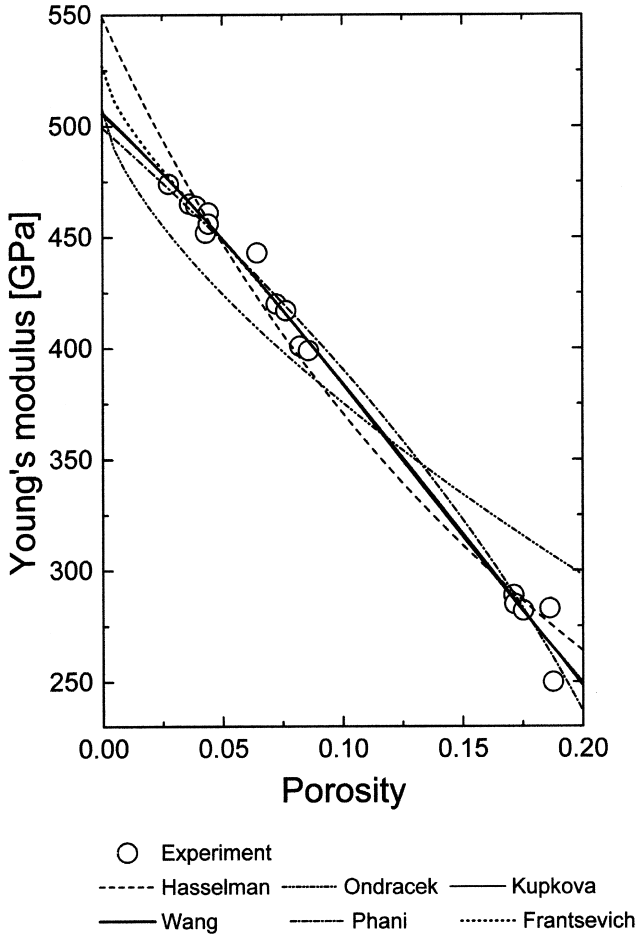

Fig. 3. Comparison of the porosity correction methods.

modulus for the non-porous state change significantly from system to system. This means that for obtaining Young's modulus at zero-porosity a set of samples with uniformly distributed porosity is necessary to calculate the accurate parameters in order to obtain appropriate results.

6. Elastic properties

6.1. Carbides

Generally the knowledge of the elastic properties is more extensive than of nitride systems. Data available of transition metal carbides deal mostly with Ti–C and Nb–C systems.

Frantsevich et al. [32] investigated the temperature dependency of Young's modulus within the temperature range of 103 to 1373 K for TiC, ZrC, VC, NbC, Cr_3C_2, Mo_2C and WC. As in general Young's modulus decreases with increasing temperature the β values obtained by Frantsevich (see Table 2) should be negative if the following formula has been used:

$$E_T = E_0(1 + \beta) \quad (27)$$

Table 2
Temperature coefficient β 10^{-6} deg^{-1} of the Young's modulus obtained by Frantsevich et al. [32]

	TiC	ZrC	VC	NbC	Cr_3C_2	Mo_2C	WC
β	80	70	120	100	130	110	69

where E_T is Young's modulus at temperature T. The samples were prepared from powders of the compounds by vacuum sintering of pressed blocks. The sintering temperatures varied from 1473 to 2873 K, but the porosity was not mentioned. Occasionally hot-pressing was employed to obtain nearly compact materials. To obtain Young's modulus for the non-porous state an equation representing the relationship between Young's modulus and porosity for porosities between 0 and 30% was used (see Eq. (28) and Eq. (29))

$$E_0 = E_0'\left[1 + a\left(\frac{P}{100}\right)^b\right] \quad (28)$$

$$E_0' = \frac{E}{\left[1 - \left(\frac{P}{100}\right)^{2/3}\right]} \quad (29)$$

where E is the normal elastic modulus of samples with given volume porosity P, expressed in percentage, E_0 is the extrapolated value of the normal elastic modulus for the nonporous state and a and b are empirically determined constants representing the effects of stress concentrations, which are determined by the macroscopic structure of the materials investigated and their relaxation capacity. For TiC even the influence of porosity was investigated (see Table 4). Frantsevich et al. [32] found that all the samples, regardless of porosity, showed a linear relationship between temperature and elastic modulus, the temperature

Table 3
Legend for the literature data tables on elastic properties

Sample:	
h	hot-pressed sample
c	single crystal
d	bulk sample prepared by diffusion annealing
f	film deposited by CVD or PVD
s	sintered sample
z	bulk sample prepared by zone annealing
–	not reported
Method:	
C	calculated value
M	mechanical test
S	sound velocity
X	X-ray diffraction
E	Young's modulus
$T(E)$	investigation temperature of Young's modulus
ν	Poisson ratio
$T(\nu)$	investigation temperature of the Poisson ratio
G	data taken from a graph

Table 4
Data on elastic properties of TiC_{1-x}

Compos. [C]/[Ti]	Sample form	Porosity (%)	E (GPa)	$T(E)$ (K)	v	$T(v)$ (K)	Method	Ref.
0.33	–	–	–	–	0.27	–	C	[24]
0.50	–	–	362	–	0.23	–	C	[24]
0.56	f	–	235	–	–	–	S	[33]^{G}
0.64	f	–	239	–	–	–	S	[33]^{G}
0.67	f	–	353	–	–	–	S	[33]^{G}
0.85	–	–	440	–	–	–	–	[49]
0.91	s	0	438	–	0.17	–	S	[50]
0.94	f	–	456	–	–	–	S	[33]^{G}
	–	–	458	–	0.18	–	–	[51]
	–	–	447	–	–	–	–	[52]
0.99	f	–	648	–	–	–	S	[33]^{G}
1.00	s	–	269	–	–	–	–	[2]
	s	–	462	–	–	–	–	[2]
	–	–	450	–	–	–	–	[3]
	f	–	460	–	–	–	S	[33]
	s	–	451	–	0.17	–	S	[32]
	s	7.66	369	–	–	–	S	[32]^{G}
	s	17.38	274	–	–	–	S	[32]^{G}
	s	18.97	258	–	–	–	S	[32]^{G}
	s	21.24	243	–	–	–	S	[32]^{G}
	s	32.83	151	–	–	–	S	[32]^{G}
	s	44.48	131	–	–	–	S	[32]^{G}
	s	64.83	23	–	–	–	S	[32]^{G}
	s	67.45	14	–	–	–	S	[32]^{G}
	–	–	314	–	–	–	–	[53]
	–	1.8	439	298	–	–	–	[53]
	–	–	314	–	–	–	–	[54]
	–	–	316	–	–	–	–	[54]
	–	–	352	–	–	–	–	[54]
	–	–	310	–	–	–	–	[54]
	–	–	379	1273	–	–	–	[54]
	–	15	–	–	0.187	–	–	[54]
	–	28	–	–	0.189	–	–	[54]
	c	0	–	–	0.182	–	–	[54]
	–	–	322	–	–	–	–	[55]
	–	–	486	–	0.19	–	C	[24]
	f	–	200	–	–	–	S	[34]
	–	–	451	–	–	–	–	[42]
	–	–	370	–	–	–	–	[41]

coefficient tending to fall as the porosity of the samples diminishes. According to these investigations the variation in the temperature coefficient of the normal elastic modulus with porosity is of an exponential type.

Speck et al. [31] investigated the temperature and porosity dependence of Young's modulus and the Poisson ratio for $NbC_{0.97}$ (see Table 8). It can be seen that with increasing temperature Young's modulus starts to decrease in contrast to the Poisson ratio, where no temperature dependency could be observed. The significant influence of porosity could be seen clearly too (see Table 8). The scatter of the data available for bulk TiC is about 44% the scatter reported for bulk NbC is about 37%. Even greater is the scatter for film samples (67%), where Török [33] reported a Young's modulus of 460 GPa and Kinbara [34] just 200 GPa.

Miodownik [24] calculated Young's modulus of transition metal carbides from their assessed thermal properties relying on the well established relationships between elastic and thermal properties [25]. It is important to note that the existence of calculated values does not imply which of the various carbide structures will actually occur like VC, V_3C, CrC and Cr_3C phases which do not exist as stable phases. The data found can be seen in Tables 4–12.

6.2. Nitrides

6.2.1. Bulk samples

A great number of room temperature data can be found for the Ti–N and Zr–N systems. Wolf [12] investigated the influence of porosity on Young's modulus and the Poisson ratio using the PEO method [11] calculating Young's modulus for the non-porous state with the equation proposed by Hasselman [13] (see Eq. (21)). He found that

Table 5
Data on elastic properties of ZrC_{1-x}

Compos. [C]/[Zr]	Sample form	Porosity (%)	E (GPa)	$T(E)$ (K)	v	$T(v)$ (K)	Method	Ref.
0.89	c	0	407	–	0.187	–	–	[2]
0.94	c	0	407	–	0.187	–	–	[2]
	–	–	478	–	0.17	–	–	[50]
0.96	h	3	386	–	0.191	–	–	[2]
1.00	–	–	350	–	–	–	–	[3]
	s	–	549	–	–	–	S	[32]
	–	–	348	–	–	–	–	[53]
	–	8	318	298	0.257	298	–	[54]
	–	–	195	–	–	–	–	[54]
	–	–	480	–	–	–	–	[54]
	–	–	338	–	–	–	–	[54]
	–	–	388	–	–	–	–	[55]
	–	–	348	–	–	–	–	[42]

Table 6
Data on elastic properties of HfC_{1-x}

Compos. [C]/[Hf]	Sample form	Porosity (%)	E (GPa)	$T(E)$ (K)	v	$T(v)$ (K)	Method	Ref.
0.97	h	3.32	461	298	0.18	298	C	[57]
1.00	s	–	317	–	–	–	–	[2]
	s	–	421	–	–	–	–	[2]
	–	–	350	–	–	–	–	[3]
	–	5	424	298	0.166	298	–	[54]
	–	–	352	–	–	–	–	[42]

because of the high longitudinal and transversal velocities in transition metals, a sample thickness of at least 3 mm is necessary for the correct detection of the sound velocity signals. Furthermore, he reported that porosities of less than 5% have to be achieved (see Section 5.1), otherwise Young's modulus calculated for the non-porous state of samples originating from higher porosities will exceed the results obtained from less porous samples.

To correct for the influence of porosity Portnoi et al. [35] was the first to investigate transition metal nitrides prepared by diffusion annealing and he observed no influence of the sample thickness within the range 50 to 800 μm using the PEO method, too. The influence of texture, because diffusion causes a preferred grain orientation, or the existence of porosity induced by the diffusion process has not been investigated. Values measured by

Table 7
Data on elastic properties of vanadium carbides

Compos. [C]/[V]	Sample form	Porosity (%)	E (GPa)	$T(E)$ (K)	v	$T(v)$ (K)	Method	Ref.
0.33[a]	–	–	352	–	0.27	–	C	[24]
0.50	–	–	361	–	0.23	–	C	[24]
0.91	–	–	350	–	–	–	–	[3]
1.00[a]	s	–	434	–	–	–	–	[2]
	–	–	271	–	–	–	–	[53]
	–	–	271	–	–	–	–	[54]
	–	–	255	–	–	–	–	[54]
	–	–	269	–	–	–	–	[54]
	–	–	446	–	0.19	–	C	[24]
	–	–	422	–	–	–	–	[42]
	–	–	430	–	–	–	–	[41]
	s	–	422	–	0.32	–	S	[32]

[a] Although data were given for single-phase samples [2,24,32,41,42,53,54] vanadium carbides do not exist with these compositions.

Table 8
Data on elastic properties of NbC_{1-x}

Compos. [C]/[Nb]	Sample form	Porosity (%)	E (GPa)	$T(E)$ (K)	ν	$T(\nu)$ (K)	Method	Ref.
0.87	c	0	438	298	0.226	298	S	[56]
0.96	s	7.9	488	298	0.22	298	C	[57]
0.97	h	8	490	–	0.23	–	–	[2]
	h	–	510	–	0.21	–	–	[2]
	h	6	441	293	0.214	293	–	[31]^{G}
	h	6	437	372	0.210	372	–	[31]^{G}
	h	6	–	–	0.211	474	–	[31]^{G}
	h	6	425	519	0.214	576	–	[31]^{G}
	h	6	414	652	0.211	694	–	[31]^{G}
	h	6	408	776	0.211	790	–	[31]^{G}
	h	6	–	–	0.213	878	–	[31]^{G}
	h	6	396	954	0.209	981	–	[31]^{G}
	h	6	392	1033	0.211	1094	–	[31]^{G}
	h	6	383	1186	0.210	1186	–	[31]^{G}
	h	6	370	1370	0.210	1393	–	[31]^{G}
	h	6	365	1450	0.211	1483	–	[31]^{G}
	h	6	–	–	0.210	1574	–	[31]^{G}
	h	6	350	1672	0.209	1672	–	[31]^{G}
	h	6	–	–	0.211	1793	–	[31]^{G}
	h	6	341	1873	0.209	1873	–	[31]^{G}
	h	6	335	1986	–	–	–	[31]^{G}
	h	6	327	2068	–	–	–	[31]^{G}
	s	0	514	–	–	–	–	[31]^{G}
	s	2.76	474	–	–	–	–	[31]^{G}
	s	3.64	465	–	–	–	–	[31]^{G}
	s	3.90	464	–	–	–	–	[31]^{G}
	s	4.30	452	–	–	–	–	[31]^{G}
	s	4.42	461	–	–	–	–	[31]^{G}
	s	4.42	456	–	–	–	–	[31]^{G}
	s	6.44	443	–	–	–	–	[31]^{G}
	s	7.24	420	–	–	–	–	[31]^{G}
	s	7.64	417	–	–	–	–	[31]^{G}
	s	8.22	401	–	–	–	–	[31]^{G}
	s	8.58	399	–	–	–	–	[31]^{G}
	s	17.12	289	–	–	–	–	[31]^{G}
	s	17.16	285	–	–	–	–	[31]^{G}
	s	17.52	282	–	–	–	–	[31]^{G}
	s	18.62	283	–	–	–	–	[31]^{G}
	s	18.76	250	–	–	–	–	[31]^{G}
1.00	s	–	338	–	–	–	S	[2]
	–	–	500	–	–	–	–	[3]
	s	–	540	–	–	–	–	[32]
	–	–	338	–	–	–	–	[53]
	–	–	339	–	–	–	–	[54]
	–	–	338	–	–	–	–	[54]
	–	–	341	–	–	–	–	[54]
	–	–	338	–	–	–	–	[42]

Table 9
Data on elastic properties of TaC_{1-x}

Compos. [C]/[Ta]	Sample form	Porosity (%)	E (GPa)	$T(E)$ (K)	ν	$T(\nu)$ (K)	Method	Ref.
0.90	c	0	303	–	–	–	–	[2]
0.99	s	15.17	537	298	0.24	298	C	[57]
1.00	s	–	365	–	–	–	–	[2]
	–	–	480	–	–	–	–	[3]
	–	–	285	–	–	–	–	[53]
	–	12.7	382	298	0.172	298	–	[54]
	–	14.3	364	298	–	–	–	[54]
	–	–	629	–	–	–	–	[54]
	–	–	286	–	–	–	–	[54]
	–	–	285	–	–	–	–	[54]
	–	–	393	–	–	–	–	[54]
	–	–	285	–	–	–	–	[42]

Table 10
Data on elastic properties of chromium carbides

Compos. [C]/[Cr]	Sample form	Porosity (%)	E (GPa)	$T(E)$ (K)	ν	$T(\nu)$ (K)	Method	Ref.
0.33[a]	–	–	320	–	0.27	–	C	[24]
0.50[a]	–	–	319	–	0.23	–	C	[24]
0.66	s	–	373	–	–	–	S	[32]
0.67	s	–	386	–	–	–	–	[2]
	–	–	370	–	–	–	–	[3]
	–	–	373	–	–	–	–	[42]
	–	–	390	–	–	–	–	[41]
1.00[a]	–	–	385	–	0.19	–	C	[24]

[a] Although data were given for single-phase samples [24] chromium carbides do not exist with these compositions.

Table 11
Data on elastic properties of molybdenum carbides

Compos. [C]/[Mo]	Sample form	Porosity (%)	E (GPa)	$T(E)$ (K)	ν	$T(\nu)$ (K)	Method	Ref.
0.50	s	–	228	–	–	–	–	[2]
	s	–	530	–	–	–	S	[32]
	–	–	530	–	–	–	–	[3]
	–	–	534	–	–	–	–	[53]
	–	–	534	–	–	–	–	[54]
	–	–	225	–	–	–	–	[54]
	–	–	223	–	–	–	–	[54]
	–	–	339	–	–	–	M	[58]
	–	–	–	–	–	–	–	[42]
	–	–	230	–	–	–	–	[41]
1.00	–	–	385	–	0.19	–	C	[24]
	–	11	197	298	0.204	298	–	[54]

Portnoi et al. [35] exceed the data measured by Wolf up to 18.9% for samples of the Ti–N system and up to 17.6% for samples of the Zr–N system, due to different evaluation procedures and because Portnoi et al. [35] measured only the longitudinal wave velocity. The measurement temperature has not been stated by Portnoi et al. [35] neither by Wolf [12], but is presumably ''room temperature''.

Investigations concerning the concentration dependency of the elastic properties within the homogeneity range of Ti–N were made by Khidirov et al. [36]. Because the samples were prepared by the SHS technique the porosities

Table 12
Data on elastic properties of tungsten carbides

Compos. [C]/[W]	Sample form	Porosity (%)	E (GPa)	$T(E)$ (K)	ν	$T(\nu)$ (K)	Method	Ref.
0.50	–	–	420	–	–	–	–	[53]
	–	–	420	–	–	–	–	[54]
1.00	s	–	669	–	–	–	–	[2]
	–	–	700	–	–	–	–	[3]
	s	–	706	–	0.31	–	S	[32]
	–	–	601	–	–	–	–	[53]
	–	2.8	668	298	–	–	–	[54]
	–	–	540	–	–	–	–	[54]
	–	–	601	–	–	–	–	[54]
	–	–	519	–	–	–	–	[54]
	–	–	707	293	–	–	–	[54]
	–	–	–	–	–	–	–	[42]
	–	–	670	–	–	–	–	[41]
1.01	s	15.38	623	298	0.18	298	C	[47]

are generally high. The values obtained at 298 K calculated for the non-porous state are in agreement with that received by Portnoi et al. [35] in contrast to Timofeeva et al. [26] and to those obtained by Wolf [12]. Furthermore, the graphically presented Poisson ratios do not comply with the ones presented in the article in any way.

6.2.2. Thin film samples

Generally it can be seen that the elastic properties obtained from thin layers are different from those of bulk samples. This might be due to the following reasons [37]:

1. Differences in the thermal expansion coefficients between the film and the substrates cause stress in the films which can be reflected in the values of the lattice parameter of both CVD and PVD films.
2. High compressive stresses due to Ar incorporation are often obtained for PVD sputtered films. However, the

Table 13
Data on elastic properties of titanium nitrides

Compos. [N]/[Ti]	Sample form	Porosity (%)	E (GPa)	$T(E)$ (K)	v	$T(v)$ (K)	Method	Ref.
0.05	f	–	250	298	–	–	S	[8]
0.20	f	–	300	298	–	–	S	[8]
0.30	f	–	425	298	–	–	S	[8]
0.38	s	4.00	110	298	0.23	298	S	[36]^{G}
0.40	s	5.22	120	298	0.22	298	S	[36]^{G}
0.45	s	13.53	150	298	0.22	298	S	[36]^{G}
0.48	d	0	298	–	–	–	S	[35]
0.50	s	14.94	210	298	0.21	298	S	[36]^{G}
0.54	f	–	507	–	–	–	S	[33]^{G}
0.55	s	13.42	250	298	0.21	298	S	[36]^{G}
0.56	d	0	308	–	–	–	S	[35]
0.60	z	0	238	–	0.297	–	S	[12]
	s	12.97	290	298	0.20	298	S	[36]^{G}
0.62	z	0	234	–	0.307	–	S	[12]
0.63	z	0	234	–	0.32	–	S	[12]
0.64	z	0	248	–	0.321	–	S	[12]
0.67	d	0	355	–	–	–	S	[35]
	s	13.73	370	298	0.19	298	S	[36]^{G}
0.68	h	–	539	–	–	–	C	[26]
0.69	d	0	370	–	–	–	S	[35]
0.70	f	–	350	298	–	298	S	[8]
	z	0	290	–	0.277	–	S	[12]
0.71	z	0	301	–	0.266	–	S	[12]
0.72	d	0	380	–	–	–	S	[35]
0.76	z	0	321	–	0.257	–	S	[12]
	f	–	529	–	–	–	S	[33]^{G}
0.77	z	0	329	–	0.255	–	S	[12]
	d	0	406	–	–	–	S	[35]
0.78	s	14.91	410	298	0.19	298	S	[36]^{G}
0.79	d	0	402	–	–	–	S	[35]
0.80	f	–	450	298	–	–	S	[8]
0.81	z	0	350	–	0.275	–	S	[12]
0.82	f	–	460	298	–	–	S	[8]
	d	0	421	–	–	–	S	[35]
0.83	d	0	445	–	–	–	S	[35]
0.84	s	13.80	440	298	0.18	298	S	[36]^{G}
	f	–	582	–	–	–	S	[33]^{G}
0.85	h	–	490	–	–	–	C	[26]
0.88	d	0	471	–	–	–	S	[35]
0.92	h	4.02	484	–	0.223	298	S	[12]
	d	0	530	–	–	–	S	[35]

Table 13. Continued

Compos. [N]/[Ti]	Sample form	Porosity (%)	E (GPa)	$T(E)$ (K)	ν	$T(\nu)$ (K)	Method	Ref.
	d	0	565	–	–	–	S	
	h	–	392	–	–	–	C	[26]
0.93	h	0.82	460	–	0.225	–	S	[12]
	h	8.26	508	–	0.225	–	S	[12]
0.94	h	15.12	446	–	0.224	–	S	[12]
	f	–	593	–	–	–	S	[33]^{G}
0.95	d	0	588	–	–	–	S	[35]
0.96	d	0	577	–	–	–	S	[35]
	d	0	600	–	–	–	S	[35]
	d	0	604	–	–	–	S	[35]
0.98	s	15.15	510	298	0.18	298	S	[36]^{G}
	h	–	382	–	–	–	C	[26]
	f	–	784	–	–	–	M	[59]
	s	–	432	–	0.25	–	S	[32]
	c	–	429	–	0.19	–	C	[60]
0.99	d	0	604	–	–	–	S	[35]
1.00	–	–	251	–	–	–	S	[53]
	–	–	250	–	–	–	–	[54]
	–	44	79	–	–	–	–	[54]
	f	–	640	–	0.295	–	X	[43]
	f	–	620	–	–	–	S	[33]^{G}
	f	–	640	–	–	–	S	[33]
	c(E_{100})	0	556	–	–	–	S	[61]
	c(E_{110})	0	446	–	–	–	S	[61]
	c(E_{111})	0	418	–	–	–	S	[61]
	–	–	612	–	–	–	–	[42]
	f	–	400	–	–	–	–	[62]
1.01	f	–	655	–	–	–	S	[33]^{G}
1.02	–	–	256	–	–	–	M	[55]
1.05	f	–	674	–	–	–	S	[33]^{G}

Ar incorporation should be small even when biases in the range up to a few hundred volts are used. Poitevin et al. [38] have also shown that no Ar could be detected by Rutherford backscattering spectrometry (RBS) analysis in TiN films deposited by reactive DC sputtering with bias voltages of up to −200 V. However, even small Ar incorporations below 1% and thus below the detection limit for RBS, can cause considerable compressive stresses, as shown by Pan et al. [39] for TiC films.

3. Incorporation of N_2 interstitially into the lattice in tetrahedral positions should result in an expansion of the lattice of PVD films. Non-equilibrium growth conditions, such as at high biases, high rates or low temperatures, could force the nitrogen to occupy these positions. This could also explain the high [N]/[Ti] ratios often found in thin film samples. Furthermore, density values about 10% above bulk values have been measured for TiN when biases above 100 V were used [40].
4. Internal stresses, generated by a high density of grain boundaries and defects such as dislocations, are normally found in PVD thin films. Stresses generated by grain boundaries may cause an expansion of the lattice since the generation and mobility of dislocations is low at low temperatures in carbides and nitrides [2].

The data given for stoichiometric TiN varies from 79 GPa [2,41] for a sample with a porosity of 44% to 612 GPa for a bulk sample [42] and 640 for a film sample [43]. The data found for nitrides are listed in Tables 13–18 (data for higher order systems are listed in Table 19). As an example and in order to visualize the data scatter the data for TiN are summarized also in Fig. 1. It can be seen that values from the same author(s) are sometimes quite consistent (increasing E with increasing [N]/[Ti] ratio). However, due to inappropriate sample characterization, different measurement and evaluation techniques and influences on the substrate, it is not possible to conclude that this different behavior stems only from the different

Table 14
Data on elastic properties of δ-ZrN_{1-x}

Compos. [N]/[Zr]	Sample form	Porosity (%)	*E* (GPa)	*T*(*E*) (K)	*ν*	*T*(*ν*) (K)	Method	Ref.
0.54	d	0	356	–	–	–	S	[35]
0.68	d	0	359	–	–	–	S	[35]
0.73	z	0	284	–	0.27	–	s	[12]
0.77	H	–	304	–	–	–	C	[26]
	d	0	270	–	–	–	M	[63]^{G}
0.79	z	0	308	–	0.261	–	S	[12]
0.80	z	0	309	–	0.277	–	S	[12]
0.82	z	0	322	–	0.254	–	S	[12]
	z	0	302	–	0.286	–	S	[12]
	d	0	290	–	–	–	M	[63]^{G}
0.83	z	0	325	–	0.258	–	S	[12]
0.85	z	0	325	–	0.246	–	S	[12]
	d	0	441	–	–	–	S	[35]
	d	0	305	–	–	–	M	[63]^{G}
0.86	h	–	333	–	–	–	C	[26]
0.89	h	3.38	428	–	0.255	–	S	[12]
	h	3.45	427	–	0.256	–	S	[12]
	d	0	488	–	–	–	S	[35]
0.90	h	3.65	431	–	0.256	–	S	[12]
	h	6.05	448	–	0.257	–	S	[12]
	h	3.74	408	–	0.252	–	S	[12]
	d	0	495	–	–	–	S	[35]
0.91	h	3.65	431	–	0.256	–	S	[12]
	d	0	340	–	–	–	M	[63]^{G}
0.95	d	0	500	–	–	–	S	[35]
	d	0	360	–	–	–	M	[63]^{G}
0.99	d	0	500	–	–	–	S	[35]
	d	0	500	–	–	–	S	[35]
	h	–	343	–	–	–	C	[26]
1.00	f	–	500	–	–	–	S	[33]^{G}
	f	–	441	–	–	–	S	[33]^{G}
	f	–	460	–	–	–	S	[33]
	s	–	392	–	0.25	–	S	[32]
	f	–	460	–	0.186	–	X	[43]
	–	–	460	–	–	–	–	[42]
1.11	f	–	395	–	–	–	S	[33]^{G}
1.12	f	–	428	–	–	–	S	[33]^{G}

state of the samples (thin film, bulk, . . .). The latter has been indicated in the legend.

Attar et al. [44] measured the stress of chromium nitride samples at different applied loads using the four-point bending test with the help of the X-ray diffraction measurements. The goniometer was equipped with Cr Kα radiation and a position sensitive detector. The diffraction peaks were fitted with the pseudo-Voight function [45] to determine the exact 2θ position. The crystallographic orientation (texture) of the chromium nitride coating was then quantitatively analyzed using the Schulz reflection method, a Seifert-PTS goniometer and a scintillation detector.

6.3. Carbonitrides

Little data can be found for transition metal carbonitride

Table 15
Data on elastic properties of δ-HfN_{1-x}

Compos. [N]/[Hf]	Sample form	Porosity (%)	*E* (GPa)	*T*(*E*) (K)	*v*	*T*(*v*) (K)	Method	Ref.
0.74	h	1.16	344	–	0.265	–	S	[12]
0.76	h	1.10	354	–	0.266	–	S	[12]
0.82	h	1.26	360	–	0.264	–	S	[12]
0.84	z	0	338	–	0.280	–	S	[12]
0.86	f	–	341	–	–	–	S	[33][G]
0.87	h	3.02	392	–	0.260	–	S	[12]
0.88	z	0	340	–	0.295	–	S	[12]
	f	–	412	–	–	–	S	[33][G]
0.89	f	–	376	–	–	–	S	[33][G]
0.93	f	–	367	–	–	–	S	[33][G]
0.94	h	4.08	459	–	0.248	–	S	[12]
0.98	h	24.63	387	–	0.259	–	S	[12]
1.00	f	–	380	–	–	–	S	[33]
	h	–	333	–	–	–	C	[26]
	f	–	380	–	0.35	–	X	[43]
	–	–	–	–	–	–	–	[42]
1.11	f	–	336	–	–	–	S	[33][G]

Table 16
Data on elastic properties of δ-VN_{1-x}

Compos. [N]/[V]	Sample form	Porosity (%)	*E* (GPa)	*T*(*E*) (K)	*v*	*T*(*v*) (K)	Method	Ref.
0.98	h	–	382	–	–	–	C	[26]
1.00	c(100)	0	478	–	–	–	S	[61]
	c(100)	0	368	–	–	–	S	[61]
	c(111)	0	342	–	–	–	S	[61]

Table 17
Data on elastic properties of δ-NbN_{1-x}

Compos. [N]/[Nb]	Sample form	Porosity (%)	*E* (GPa)	*T*(*E*) (K)	*v*	*T*(*v*) (K)	Method	Ref.
0.95	h	–	373	–	–	–	C	[26]
1.00	c(100)	0	490	–	–	–	S	[61]
	c(110)	0	357	–	–	–	S	[61]
	c(111)	0	328	–	–	–	S	[61]

Table 18
Data on elastic properties of chromium nitrides

Compos. [N]/[Cr]	Sample form	Porosity (%)	*E* (GPa)	*T*(*E*) (K)	*v*	*T*(*v*) (K)	Method	Ref.
0.50	s	–	314	–	–	–	S	[32]
0.97	s	–	324	–	0.26	–	S	[32]
1.00	f	–	520	–	0.214	–	X	[44]
	f	–	452	–	0.199	–	X	[44]
	f	–	441	–	0.207	–	X	[44]
	–	–	461	–	0.264	–	X	[44]
	f	–	400	–	–	–	–	[64]
	f	–	232	–	–	–	–	[65]
	f	–	244	–	–	–	–	[65]

Table 19
Data on elastic properties of higher order systems

Composition	Sample form	Porosity (%)	E (GPa)	$T(E)$ (K)	ν	$T(\nu)$ (K)	Method	Ref.
$(Ta_{0.67}Zr_{0.33})C$	–	–	113	298	0.18	298	–	[54]
$(Ta_{0.87}Zr_{0.2})C$	–	8.9	406	298	–	–	–	[54]
	–	22.2	231	298	–	–	–	[54]
	–	11.1	–	–	0.212	298	–	[54]
$(Ta_{0.89}Zr_{0.11})C$	–	7.7	363	298	0.151	298	–	[54]
$(Ta_{0.8}Hf_{0.2})C$	–	16.7	403	298	0.219	298	–	[54]
	–	31	221	298	–	–	–	[54]
Cr_3C_2–WC	h	–	385	–	–	–	–	[66]
$(V_{0.06}Nb_{0.4})N$	f	–	857	–	–	–	M	[59]
$(Ti_{0.3}V_{0.42}Nb_{0.28})N$	f	–	881	–	–	–	M	[59]

systems. Ivanov et al. [46] investigated the influence of the [C]/[N] ratio on the elastic properties of the Ti–C–N system, whereas Borisov et al. [47] obtained the concentration-dependent elastic properties for Ti–M–C–N systems, where M stands for Zr, Hf, V or Nb.

The samples prepared by Ivanov et al. [46] were obtained by sintering at 1873 K for 16 h and subsequent vacuum hot-pressing. Therefore, the porosities were ranging from 4.9 to 18.6%, but mostly larger than 12%. He found that by replacing the C by N atoms Young's modulus, calculated from the longitudinal and transverse wave velocities, starts to decrease first reaching a minimum near the composition $TiC_{0.61}N_{0.31}$ and then rising again forming a flat maximum. Data obtained by Manghnani [48] on less porous samples exceed the data obtained by Ivanov et al. [46] due to a higher C and N concentration, different evaluation methods and a different measurement temperature.

Borisov et al. [47] investigated the concentration dependence of the microhardness and the elastic properties in Ti–M–C–N systems, where M stands for Zr, Hf, V or Nb. The compact polycrystalline specimens were obtained by hot-pressing in Argon atmosphere at 2073–2673 K. The final porosity of the samples was stated to be between 1.5 and 8%, but not mentioned in detail for the various systems studied. In his investigations he observed several characteristic regions. In all systems, except the Ti–Hf–C–N system, maxima at 10–40 mol% M–N and 60 mol% M–N and a minimum at an equimolar ratio of Ti–C to M–N is reported. According to Borisov et al. [47] the appearance of extrema is due to a redistribution of the electron density, which leads to a strengthening of the M–N bond in comparison with the Ti–C bonds by the replacement of Ti and C atoms by M and N atoms and, on the other hand as in case of binary metallic systems, a stronger Ti–M bond appears leading to an increase of the elastic property values. The presence of a second maximum may be due to a short-range ordering effect of metal atoms in quaternary solid solutions. In contrast to Young's modulus the Poisson ratio changes monotonically with the MN content.

Because of the few data available for transition metal carbonitride systems (see Table 20 and Table 21) no comparison of the values can be made.

Table 20
Data on elastic properties of hot-pressed TiC–ZrN, TiC–HfN, TiC–NbN or $TiC_{0.5}N_{0.5}$–VC systems reported by Borisov et al. [47] obtained by sound measurements. Porosity between 1.5% and 8%, but as well as the measurement temperature not stated specifically. Data taken from a graph.

mol% ZrN	E (GPa)	ν	mol% HfN	E (GPa)	ν	mol% NbN	E (GPa)	ν	mol% VC	E (GPa)	ν
0.0	460	0.17	0.0	460	0.17	0.0	460	0.17	0.0	430	0.17
0.2	500	0.19	0.2	460	0.17	0.2	470	0.19	0.2	540	0.22
0.4	480	0.20	0.4	560	0.20	0.3	480	–	0.4	470	0.21
0.5	430	0.21	0.5	580	0.21	0.4	480	0.20	0.5	450	0.20
0.6	460	0.22	0.6	550	0.20	0.5	460	0.22	0.6	480	0.20
0.8	430	0.23	0.8	410	0.25	0.6	490	0.23	0.8	440	0.21
1.0	340	0.22	1.0	500	0.28	0.8	460	0.24			
						1.0	400	0.26			

Table 21
Data on elastic properties of hot-pressed titanium carbonitrides

Composition	Sample form	Porosity (%)	E (GPa)	$T(E)$ (K)	ν	$T(\nu)$ (K)	Method	Ref.
$TiC_{0.86}N_{0.10}$	h	4.9	440	290	0.160	290	S	[46]^{G}
$TiC_{0.82}N_{0.15}$	h	14.8	420	290	0.164	290	S	[46]^{G}
$TiC_{0.70}N_{0.23}$	h	16.8	400	290	0.154	290	S	[46]^{G}
$TiC_{0.61}N_{0.31}$	h	18.6	400	290	0.162	290	S	[46]^{G}
$TiC_{0.53}N_{0.40}$	h	16.4	400	290	0.157	290	S	[46]^{G}
$TiC_{0.41}N_{0.50}$	h	12.2	410	290	0.178	290	S	[46]^{G}
$TiC_{0.40}N_{0.60}$	h	3.3	459	298	0.212	298	S	[48]
$TiC_{0.33}N_{0.58}$	h	9.3	430	290	0.189	290	S	[46]^{G}
$TiC_{0.20}N_{0.80}$	h	3.5	451	298	0.212	298	S	[48]
$TiC_{0.14}N_{0.77}$	h	7.1	410	290	0.197	290	S	[46]^{G}
$TiC_{0.04}N_{0.87}$	h	12.0	370	290	0.208	290	S	[46]^{G}

Acknowledgments

The authors would like to thank Prof. M.H.Manghnani of the University of Hawaii at Manoa, USA for performing the sound velocity measurements of TiCN samples and Mr. Klaus Krämer, KSI, Herborn, Germany for supplying an acoustic microscope investigation on a HfCN sample. This work was supported by the Austrian National Science Foundation (FWF) under project No. 11892-PHY.

References

[1] E.K. Storms, Refractory Carbides, Academic, New York, 1968.
[2] L.E. Toth, Transition Metal Carbides and Nitrides, Academic, New York, 1971.
[3] P. Ettmayer, W. Lengauer, Carbides: Transition metal solid-state chemistry, in: Encyclopedia of Inorganic Chemistry, Wiley, New York, 1994, p. 519–531.
[4] P. Ettmayer, W. Lengauer, Nitrides: Transition metal solid-state chemistry, in: Encyclopedia of Inorganic Chemistry, Wiley, New York, 1994, p. 2498–2514.
[5] H. Matzke, Defect and Diffusion Forum 83 (1992) 111.
[6] M. Wittmer, B. Studer, H. Melchior, J. Appl. Phys. 52 (1981) 5722.
[7] M.A. Nicolet, Thin Solid Films 52 (1978) 415.
[8] X. Jiang, M. Wang, K. Schmidt, E. Dunlop, J. Haupt, W. Gissler, J. Appl. Phys. 69(5) (1991) 3053.
[9] H.J. McSkimin, IRE Trans. PGUE 5 (1957) 251.
[10] I. Jackson, H. Niesler, The elasticity of periclase to 3 GPA and some geophysical applications in high-pressure research in geophysics, in: S. Akimoto, M.H. Manghnani (Eds.), Advances in Earth and Planetary Sciences, Reidel Pub. Co., 1982, p. 93–113.
[11] D.H. Chung, D.J. Silversmith, B.B. Chick, Rev. Sci. Instruments 40 (1969) 718.
[12] T. Wolf, Thesis, Herstellung und Charakterisierung von TiN, ZrN und HfN, University of Karlsruhe, 1982.
[13] D.P.H. Hasselman, J. Am. Ceram. Soc. 45 (1962) 452.
[14] G. Ondracek, Proc. Colloquium Brussels, 1988.
[15] M. Kupkova, J. Mater. Sci. 28 (1993) 5265.
[16] J.C. Wang, J. Mater. Sci. 19 (1984) 801.
[17] K.K. Phani, S.K. Niyogi, J. Mater. Sci. 22 (1987) 257.
[18] T. Mori, K. Tanaka, Acta Metall. 21 (1973) 571.
[19] S.P. Timoshenko, J.N. Goodier, in: Theory of Plasticity, 3rd ed., Mc Graw Hill, New York, 1969.
[20] D. Rafaja, V. Valvoda, A.J. Perry, J.R. Treglio, Surf. Coat. Technol., in press.
[21] F. Bollenrath, V. Hauk, E.H. Müller, Z. Metallkde 58 (1967) 77.
[22] D. Rafaja, V. Valvoda, Powder Diff. 6(4) (1991) 200.
[23] A.J.C. Wilson, Elements of X-ray crystallography, Addison-Wesley Publishing Company, Reading, 1970.
[24] A.P. Miodownik, Mater. Sci. Technol. 10 (1994) 190.
[25] G. Grimvall, J. Rosen, Int. J. Thermophys. 4(2) (1983) 139.
[26] I.I. Timofeeva, L.K. Shvedova, Inorg. Mater. 8 (1972) 1027.
[27] Y.I. Frenkel, Fizmatgiz, Moscow, 1958.
[28] J.C. Wang, J. Mater. Sci. 19 (1984) 809.
[29] K.K. Phani, J. Mater. Sci. 31 (1996) 272.
[30] A.K. Maitra, K.K. Phani, J. Mater. Sci. 29 (1994) 4415.
[31] D.A. Speck, B.R. Miccioli, Carborundum Company Report, 1968, cited in .
[32] I.N. Frantsevich, E.A. Zhurakovskii, A.B. Lyashchenko, Inorg. Mater. 3 (1967) 6.
[33] E. Török, A. Perry, L. Chollet, W.D. Sproul, Thin Solid Films 153 (1987) 37.
[34] A. Kinbara, S. Baba, Thin Solid Films 107 (1983) 359.
[35] K.I. Portnoi, A.A. Mukaseev, V.N. Gribkov, Y.V. Levinskii, Sov. Powder Met. Metall Ceram. 61 (1968) 406.
[36] I. Khidirov, T. Khaidarov, Inorg. Mater. 31(1) (1995) 134.
[37] J.E. Sundgren, Thin Solid Films 128 (1985) 21.
[38] J.M. Poitevin, G. Lemperiere, J. Tardy, Thin Solid Films 97 (1982) 69.
[39] A. Pan, J.E. Green, J.R. Hellmann, Thin Solid Films 78 (1981) 25.
[40] G. Lempiere, J.M. Poitevin, Thin Solid Films 111 (1984) 339.
[41] S.T. Oyama, Introduction to the chemistry of transition metal carbides and nitrides, in: S.T. Oyama (Ed.), Transition Metal Carbides and Nitrides: Application of Transition Metal Carbides and Nitrides in Industrial Tools, Blackie Acad. and Prof., London, 1996, Chap. 1, p. 1.
[42] A.T. Santhanam, Introduction to the chemistry of transition metal carbides and nitrides, in: S.T. Oyama (Ed.), Transition Metal Carbides and Nitrides: Application of Transition Metal Carbides and Nitrides in Industrial Tools, Blackie Acad. and Prof., London, 1996, Chap. 2, p. 28.
[43] A.J. Perry, Thin Solid Films 193(1–2) (1990) 463.
[44] F. Attar, T. Johannesson, Thin Solid Films 258 (1995) 205.
[45] C. Persson, Ph.D. Thesis 328, Residual stresses and mechanical properties of metal matrix composites, Linköping, 1993.
[46] N.A. Ivanov, L.P. Andreeva, S.I. Alyamovskii, B.V. Mitrofanov, Izv. Akad. Nauk SSSR, Neorg. Mater. 12 (1976) 1203.
[47] S.V. Borisov, B.V. Mitrofanov, G.P. Shveikin, Inorg. Mater. 15 (1979) 1684.
[48] M.H. Manghnani, private communications.
[49] J.L. Chermant, Rev. Int. Hautes Témp. Réfract. 6 (1969) 299.
[50] R. Chang, L.J. Graham, J. Appl. Phys. 37 (1966) 3778.
[51] J.J. Gilman, B.W. Roberts, J. Appl. Phys. 32 (1961) 1405.
[52] W.S. Williams, R.D. Schaal, J. Appl. Phys. 33 (1962) 955.

[53] S. Neshpor, G.V. Samsonov, Fiz. Met. Metalloved. 4 (1957) 181.
[54] P.T.B. Shaffer, Plenum Press Handbook of High Temperature Materials. Materials Index Plenum Press, New York, 1964, No. 1.
[55] R. Kieffer, Sondermetalle, Springer Verlag, Wien, 1971.
[56] H.M. Ledbetter, S. Chevacharoenkul, R.F. Davis, J. Appl. Phys. 60(5) (1986) 1614.
[57] H.L. Brown, P.E. Armstrong, C.P. Kempter, J. Chem. Phys. 45(2) (1966) 547.
[58] A.E. Martinelli, R.A.L. Drew, R. Berriche, J. Mater. Sci. Lett. 15 (1996) 307.
[59] K.M. Hubbard, T.R. Jervis, P.B. Mirkarimi, S.A. Barnett, J. Appl. Phys. 72(9) (1992) 4466.
[60] W.G. Sloof, B.J. Kooi, R. Delhez, T.H. de Keijser, E.J. Mittemeijer, J. Mater. Res. 11(6) (1996) 1440.
[61] J.O. Kim, J.D. Achenbach, P.B. Mirkarimi, M. Shinn, S.A. Barnett, J. Appl. Phys. 72(5) (1992) 1805.
[62] M. Wittling, A. Bendavid, P.J. Martin, M.V. Swain, Thin Solid Films 270 (1995) 283.
[63] V.P. Yanchur, R.A. Andrievskii, I.I. Spivak, M.A. Fedotov, Inorg. Mater. 5 (1969) 861.
[64] H. Holleck, J. Vac. Sci. Technol. A 4(6) (1986) 2661.
[65] J.A. Sue, A.J. Perry, J. Vetter, Proc. Int. Conf. Metallurgical Coatings and Thin Films, San Diego, CA, April, 1994.
[66] T.S. Chen, P.L. Chung, L.K. Ai, J. Mater. Sci. 31 (1996) 3475.